

# Structure–property relationship of luminescent zirconia nanomaterials obtained by sol–gel method

José M. Carvalho · Lucas C. V. Rodrigues ·  
Maria C. F. C. Felinto · Luiz A. O. Nunes ·  
Jorma Hölsä · Hermi F. Brito

Received: 30 June 2014 / Accepted: 3 October 2014 / Published online: 4 November 2014  
© Springer Science+Business Media New York 2014

**Abstract** Nanocrystalline  $\text{ZrO}_2$  materials were prepared by sol–gel method combining different  $W = [\text{H}_2\text{O}]/[\text{ZTB}]$  ratios (ZTB: zirconium tetrabutoxide) with 600, 800, and 1000 °C annealing temperatures, yielding diverse phase compositions. A lower post-synthesis annealing temperature (600 °C) favored the  $t\text{-ZrO}_2$  tetragonal phase while higher temperatures (800 and 1000 °C) yielded the monoclinic one ( $m\text{-ZrO}_2$ ). Depending on the preparation conditions, mixed structure materials are readily obtained. The luminescence activator in the undoped  $\text{ZrO}_2$  is assumed as trivalent titanium and emission bands are assigned to the  $3d^1(e_g) \rightarrow 3d^1(t_{2g})$  transition. Due to weaker crystal field in  $m\text{-ZrO}_2$  form, the  $\text{Ti}^{3+}$  emission band is red-shifted from 410 nm in  $t\text{-ZrO}_2$  to 500 nm. The luminescence intensity of the  $t\text{-ZrO}_2$  form is quenched at

higher temperature than that of  $m\text{-ZrO}_2$ , indicating higher activation energy and smaller Stokes shift. The undoped  $\text{ZrO}_2$  excitation seems to involve photoionization of  $\text{Ti}^{3+}$  to  $\text{Ti}^{\text{IV}}$ . Simultaneously, the freed electron is trapped to the oxygen vacancies ( $\text{F}^{++}$  centers) created by  $\text{Ti}^{3+}/\text{Ti}^{\text{IV}}$  charge compensation, so this can be considered as a metal-to-host/ligand charge transfer. Since most of the excitation results in immediate emission, the traps are probably very shallow though deeper ones leads to the persistent luminescence from the undoped  $\text{ZrO}_2$ .

## Introduction

$\text{ZrO}_2$  is one of the most important metal oxides with applications in photonic devices due to several unique properties such as good thermal and chemical stability [1], high refractive index (2.15–2.18) [2], and low phonon energy [3]. The Zr–O stretching frequency is ca.  $470 \text{ cm}^{-1}$ , which is much lower than for Al–O (870) or Si–O (1100) while higher than for Y–O (300–380) [4]. The wide band gap of  $\text{ZrO}_2$  (5.0–5.5 eV) is important for the use as luminescent materials providing good optical transparency [5]. In addition to the photonic materials, zirconia has a variety of other applications, including thermal barrier coatings [2], fuel cell electrolytes [6], catalysis [7], and oxygen sensors [8].  $\text{ZrO}_2$  shows a well-known polymorphism with three different crystal structures: cubic ( $c\text{-ZrO}_2$ ), tetragonal ( $t\text{-ZrO}_2$ ), and monoclinic ( $m\text{-ZrO}_2$ ) [9]. The point symmetry of the Zr site is  $\text{C}_{2h}$  and  $\text{D}_{4h}$  for the monoclinic and tetragonal form, respectively, indicating that the local monoclinic structure is less symmetric than tetragonal as well. Although  $m\text{-ZrO}_2$  is stable at room temperature, yet it is transformed to the tetragonal phase at 1250 °C, and then to cubic at 2370 °C [10]. Nevertheless,

J. M. Carvalho · L. C. V. Rodrigues · J. Hölsä · H. F. Brito (✉)  
Instituto de Química, Universidade de São Paulo, Av. Prof.  
Lineu Prestes, 748, São Paulo, SP, Brazil  
e-mail: hefbrito@iq.usp.br

J. Hölsä  
e-mail: jholasa@utu.fi

L. C. V. Rodrigues · J. Hölsä  
Department of Chemistry, University of Turku, 20014 Turku,  
Finland

M. C. F. C. Felinto  
Instituto de Pesquisas Energéticas e Nucleares, Av. Prof. Lineu  
Prestes, 2242, São Paulo, SP, Brazil

L. A. O. Nunes  
Instituto de Física de São Carlos, Universidade de São Paulo,  
Av. Trabalhador São-Carlense, 400, São Carlos SP, Brazil

J. Hölsä  
Turku University Centre for Materials and Surfaces (MatSurf),  
Turku, Finland

the tetragonal and cubic phases can be stabilized at the room temperature by doping with trivalent rare earth ( $R^{3+}$ ) and divalent alkaline earth ( $Mg^{2+}$  and  $Ca^{2+}$ ) ions, generating oxygen vacancies as a result of charge compensation [11–13]. Even sulfur impurities have been used to stabilize the cubic form [14].

The luminescence of the  $ZrO_2$  materials has been studied extensively, mainly when doped with the  $R^{3+}$  ions, including the energy transfer from the host to the doping ion [15, 16]. The intrinsic luminescence of the undoped zirconia materials has also been observed in different works though the origin of this emission is still basically an open question. Numerous hypotheses concerning the emission from undoped zirconia have been given in the literature including the self-activation of Zr caused by an asymmetric coordination of the oxygen atoms [17], and the point defects in the zirconia structure [5, 10, 18]. Eventually, it has been suggested that the luminescence comes from Ti present in the crystal lattice as an impurity [19, 20]. The luminescence of the Ti-doped  $ZrO_2$  has been attributed to the activation of  $Ti^{IV}$  in the zirconia lattice. This interpretation originated from the observation that the undoped zirconia presented the same spectroscopic behavior as with Ti doping. The earlier mechanisms for the conventional and persistent luminescence based on the presence of Ti in  $ZrO_2$  are, however, rather qualitative [21] and do not account for *e.g.* the energetics in the system. In a later work, both the conventional and persistent luminescence of undoped  $ZrO_2$  was suggested to result from a  $Ti^{3+}$  impurity in  $ZrO_2$  [22].

In this work, nanocrystalline  $ZrO_2$  materials were prepared by sol–gel method combining different  $W = [H_2O]/[ZTB]$  ratios (ZTB: zirconium tetrabutoxide) with three annealing temperatures (600, 800, and 1000 °C) to obtain different tetragonal and monoclinic phase compositions. The photoluminescence arising from different polymorphs of zirconia was correlated with the different crystal field splitting of the 3d1 configuration of  $Ti^{3+}$ .

## Experimental

### Materials preparation

1-butanol (99.5 %) and zirconium tetrabutoxide (ZTB, 70 wt%, 1-butanol solution) were purchased from Aldrich and used as received. The  $ZrO_2$  nanomaterials were prepared using a conventional sol–gel method [23], where the ZTB was hydrolyzed with different amounts of deionized water according to the ratio  $W = [H_2O]/[ZTB] = 3, 4, 5, 6, 8,$  and 10. In a typical synthesis, 4 cm<sup>3</sup> of ZTB was added in a round bottomed flask containing 25 cm<sup>3</sup> of 1-butanol. The homogeneous solution was capped and stirred for 15 min, and then water was added dropwise. The gel-like solution

was allowed to react for 24 h at room temperature. The crude gel then was dried at 110 °C for 12 h. In the next step, the dried gel was ground in a mortar and a white finely divided powder was obtained. These as-prepared materials were further annealed at 600, 800, and 1000 °C for 5 h.

### Apparatus

Thermogravimetric analyses were carried out with a Mettler-Toledo TG/SDTA 822 thermobalance, using platinum crucibles containing ca. 10 mg of the sample, under synthetic air atmosphere (flow rate: 50 cm<sup>3</sup> min<sup>-1</sup>), using a heating rate of 10 °C min<sup>-1</sup>. The infrared absorption spectra of the materials were measured with a Bomem MB102 FT-IR spectrometer in the range of 400–4000 cm<sup>-1</sup> with 4 cm<sup>-1</sup> as the spectral resolution. The crystal structure of the materials was routinely verified with the X-ray powder diffraction (XPD) measurements using a Rigaku Miniflex diffractometer with  $CuK_{\alpha 1}$  radiation (1.5406 Å) between 20 and 65° (in 2θ) with 0.05 degree 2θ step and 0.5 s step time. The Scherrer equation:

$$d = \frac{K \times \lambda}{\beta \times \cos \theta} \quad (1)$$

$$\beta^2 = \beta_S^2 - \beta_R^2 \quad (2)$$

was used to calculate the mean crystallite size  $d$ . In this expression (Eq. 1),  $K$  is the form factor (0.9 rad),  $\lambda$  the wavelength of the X-ray radiation (1.5406 10<sup>-10</sup> m), and  $\beta$  the full width at half maximum (FWHM) value (rad) of the ( $\bar{1}11$ ) diffraction reflection (at 28.2° in 2θ). The reflection broadening due to the diffractometer setup was eliminated from the  $\beta_S$  value (Eq. 2) using a microcrystalline sodium chloride as reference ( $\beta_R$ ). However, it should be realized that the Scherrer equation (Eq. 1) can be applied only to materials with an average crystal size of less than ca. 200 nm. The phase percentage ( $X_m$ ) was determined by the formula (Eq. 3) [24]:

$$X_m = \frac{I_m(111) + I_m(\bar{1}11)}{I_m(111) + I_t(101) + I_m(\bar{1}11)} \quad (3)$$

where  $I_m$  and  $I_t$  are the integrated intensities of the appropriate reflections for the monoclinic and tetragonal phases, respectively.

The scanning electron microscopy imaging (SEM) of the  $ZrO_2$  materials prepared with different  $W$  was carried out with a JEOL JSM-740 1F Field Emission Scanning Electron Microscope.

The photoluminescence measurements on the zirconia materials were carried out at room temperature with a SPEX Fluorolog-2 spectrofluorometer equipped with two 0.22 m SPEX 1680 double grating monochromators. A 450 W xenon lamp was used as the excitation source. The

excitation and emission spectra were collected at an angle of  $22.5^\circ$  (front face). All spectra were recorded using automatic correction against spectral sensitivity of detection. Temperature dependent spectra were measured using a liquid  $N_2$  cryostat with homemade temperature controller operating from 77 to 400 K.

## Results and discussion

### Phase formation and morphology of sol–gel derived $ZrO_2$

The TG curve of a representative as-prepared  $ZrO_2$  material ( $W$ : 3) shows a mass loss at three main stages in the temperature intervals of 30–110, 110–265, and 265–480  $^\circ C$  (Fig. 1). The first stage is probably due to loss of water and solvent adsorbed and trapped in the pores of the dried gel [25]. The second one is compatible with an oxidative decomposition of residual organic moiety while the third stage is related to the dehydroxylation of  $ZrOH$  and formation of  $ZrO_2$  [25]. The final composition of the material was achieved at ca. 500  $^\circ C$ . No considerable differences were observed on the thermal decomposition behavior of the materials obtained with different  $W$ .

The FT-IR absorption spectra of the as-prepared  $ZrO_2$  materials (not shown here) present a broad band at ca.  $3400\text{ cm}^{-1}$  and a narrower one at  $2900\text{ cm}^{-1}$ , assigned to the O–H and C–H stretching vibrations of water and butanol, respectively, present as residues of the sol–gel process. The FT-IR results support the analysis of the TG curves. Furthermore, the absorption bands at 480 and  $620\text{ cm}^{-1}$  are assigned to the Zr–O and Zr–OH stretching vibrations, respectively.

All XPD patterns of the  $ZrO_2$  materials prepared with  $W$ : 3 and 6, and annealed at 600, 800, and 1000  $^\circ C$  show

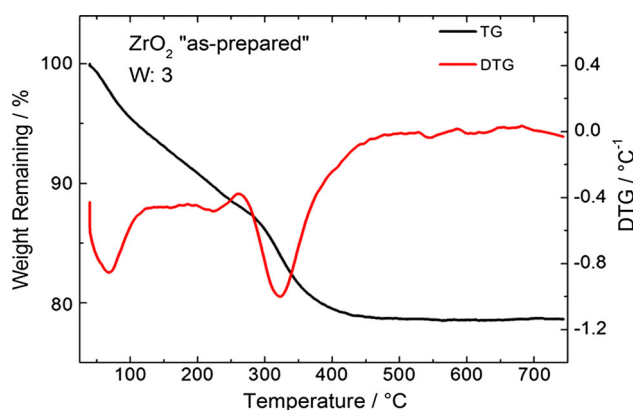


**Fig. 1** TG and DTG curves of the as-prepared  $ZrO_2$  material obtained in air atmosphere, at a heating rate of  $10\text{ }^\circ C\text{ min}^{-1}$  and flow rate at  $50\text{ cm}^3\text{ min}^{-1}$

narrow reflections which indicate the high crystallinity of the materials (Fig. 2). The most intense reflections at  $28.2$  and  $31.5^\circ$  (in  $2\theta$ ) correspond to the  $(\bar{1}11)$  and  $(111)$  reflections of the monoclinic phase (space group  $P2_1/c$ ;  $Z$ : 4) [26], respectively, whereas that at  $30.2^\circ$  corresponds to the  $(101)$  reflection of the tetragonal phase (space group  $P4_2/nmc$ ;  $Z$ : 2) [26]. The sol–gel method using different  $W$  ratios allowed the preparation of zirconia materials with different proportions between the tetragonal and monoclinic phases after the thermal treatment.

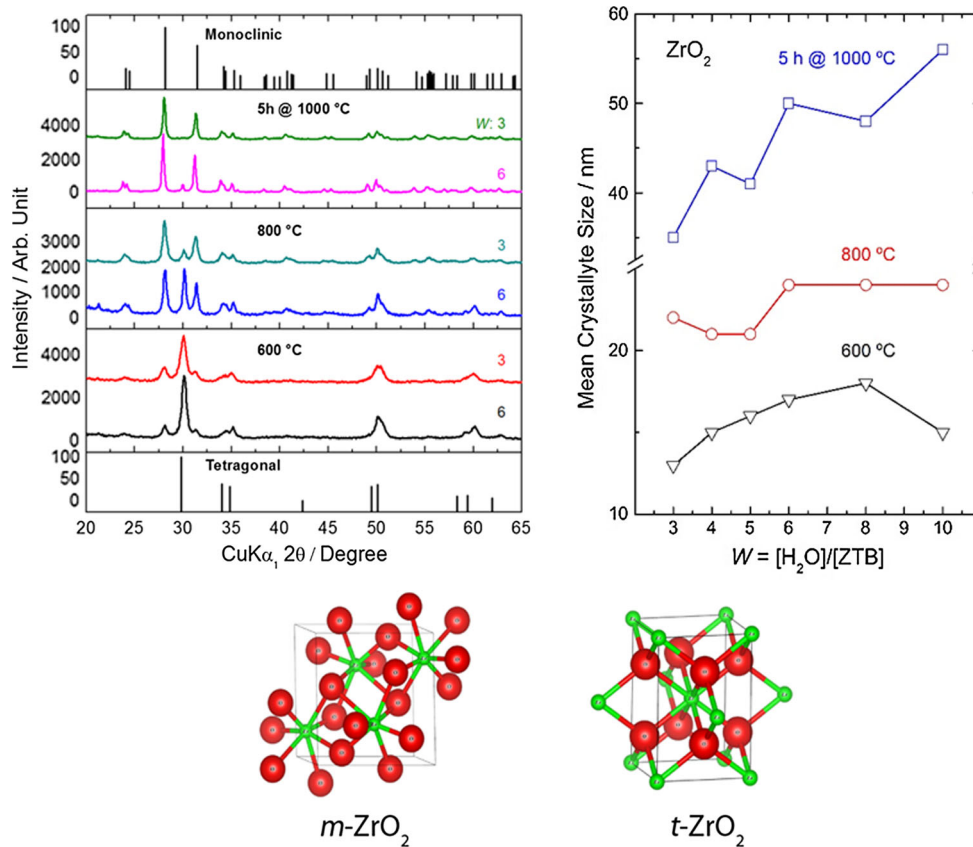
The XPD patterns of the  $ZrO_2$  materials annealed at 600  $^\circ C$  (Fig. 2) indicate that the tetragonal phase is dominant at low temperatures. Tetragonal phase is thermodynamically unstable in the case of chemically pure bulk zirconia. But in the case of (a) small particle size or (b) certain impurities ( $Y_2O_3$ , etc.), the tetragonal phase can become thermodynamically stable already at room temperature. Tetragonal phase present is then attributed to the method of synthesis which yields small particles that stabilize  $t$ - $ZrO_2$  by excess of surface energy [27]. The hydrolysis of the sol–gel zirconia precursor (ZTB) could be controlled to generate ordered sheets of  $Zr(OH)_4 \cdot 2H_2O$  that lead to the tetragonal phase upon heating [11]. Theoretical investigation on the relative stabilities of the  $ZrO_2$  crystalline phases present in the literature [28] has shown a good agreement with the obtained experimental data. The present results suggest direct influence of the  $W$  ratio on the zirconia phases, with the  $W$ : 3 ratio offering the best synthetic condition for the crystallization of the monoclinic phase (Fig. 2). On the other hand, with increasing annealing temperature, the monoclinic phase becomes predominant at 800 and 1000  $^\circ C$ , indicating a  $t \rightarrow m$  transition to the thermodynamically stable phase [11]. The mean crystallite size of  $ZrO_2$  (Fig. 2) at the annealing temperature of 600, 800, and 1000  $^\circ C$ , respectively, indicates a significant increase in the crystallite size with the increasing  $W$  ratio. Even stronger dependence of the crystalline size is shown by an increase in the annealing temperature from 600 to 1000  $^\circ C$  (Fig. 2), a well-known tendency.

SEM images show that the agglomeration and the shape of the particles for the as-prepared  $ZrO_2$  materials (Fig. 3) obtained with  $W$ : 3 and 6 depend on the water content in the synthesis. For  $W$ : 3 (Fig. 3a, b), the particles have a wide size distribution and are highly agglomerated. On the contrary, for  $W$ : 6 (Fig. 3b, c) the particles have diameter around 0.7  $\mu m$ , and are less agglomerated.

### Structural dependence of $ZrO_2$ photoluminescence

Approximately 20 different metal impurities may be present in zirconia materials in ppm concentrations [20], depending on the source. Among the proved impurities,

**Fig. 2** X-ray powder diffraction patterns of the  $ZrO_2$  materials annealed at 600, 800 and 1000 °C for  $W$  values of 3 and 6. Vertical bars indicate the standard PDF data for the monoclinic and tetragonal phases [26] (Left). The schematic presentation of the structures of  $m$ - $ZrO_2$  and  $t$ - $ZrO_2$  with 7 and 8 coordinated Zr, respectively (below). Mean crystallite size as a function of the  $W$  ratio for sol–gel zirconia materials annealed at different temperatures (right)



titanium is one of the best candidates to exhibit luminescence, and from the different Ti species, the  $Ti^{3+}$  ion may be preferred. Therefore, the luminescence from the  $ZrO_2$  materials could be improved with an addition of different amounts of the Ti dopant [19, 20], but the oxidation state of Ti could not be resolved. According to the Vegard's rule [29], it is more likely that the  $Ti^{3+}$  (ionic radius: 0.67 Å for CN: 6) substitutes  $Zr^{IV}$  (0.78/0.84 Å, CN: 7/8) in the  $ZrO_2$  lattice than  $Ti^{IV}$  (0.61/0.74 Å, CN: 6/8) [30]. Moreover, the luminescence of  $Ti^{3+}$  has been reported in matrices as aluminosilicate glass [31, 32] and bazirite-type  $BaZr_{1-x}Ti_xSi_3O_9$  phosphors [33].

The UV-excited emission spectra of the representative  $ZrO_2$  materials ( $W$ : 3) annealed at 800 and 1000 °C differ significantly from that of the material annealed at 600 °C (Fig. 4). These spectra are in good agreement with the literature data [30, 31], indicating different broad emission bands with emission centered at ca. 410 and 500 nm, respectively. The materials exhibit either bright blue (tetragonal) or cyan emission (monoclinic) colors. Considering the  $Ti^{3+}$  ion as the luminescent activator, it is expected that the tetragonal (CN: 8) and monoclinic (CN: 7) phases present different emission bands, since the  $d$ -transition metal ions are very sensitive to the crystalline field.

The excitation spectra of  $ZrO_2$  materials (Fig. 5) obtained by monitoring the emission at either 410 or 500 nm for the samples annealed at 600 and 800/1000 °C show broad absorption bands composed with two Gaussian contribution each. The higher intensity of the deconvolution curves of the excitation bands of the  $ZrO_2$  materials (Fig. 5, top) prepared at 600 °C shows a major contribution centered at 29000  $cm^{-1}$  assigned mainly to the  $d-d$  intra-configurational transition of  $Ti^{3+}$  in a tetragonal site. The deconvoluted excitation spectra of  $ZrO_2$  materials obtained at 800/1000 °C present two contributions centered at 34000 and 31800  $cm^{-1}$  attributed to the charge transfer from  $Ti^{3+}$  to the host, and  $d-d$  excitation of  $Ti^{3+}$  in a monoclinic site, respectively. It is possible to observe the contribution of the charge transfer band with lower intensity in the tetragonal phase. Generally, the charge transfer transition is independent of the environment around the  $Ti^{3+}$  and may not be attributed to an excitation to a higher  $3d^1(e_g)$  level. A more plausible explanation is offered by a transition originating from a charge (electron) transfer from  $Ti^{3+}$  to an oxygen vacancy, which was created by the charge compensation due to the  $Ti^{3+}$  impurity. The electron transfer from  $Ti^{3+}$  creates a tetravalent titanium species with a reasonably low amount of energy as should be expected.

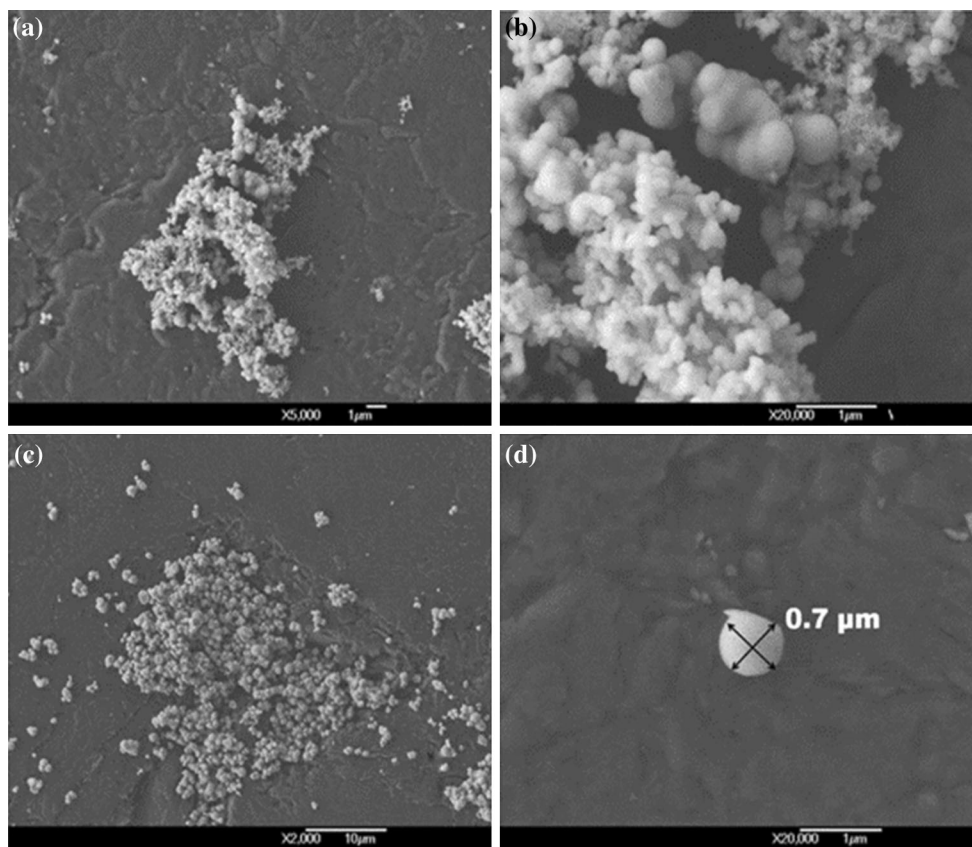


**Fig. 3** SEM images of the as-prepared ZrO<sub>2</sub> materials with magnification of **a** 5000 and **b** 20000 for W: 3; **c** 2000 and **d** 20000 for W: 6

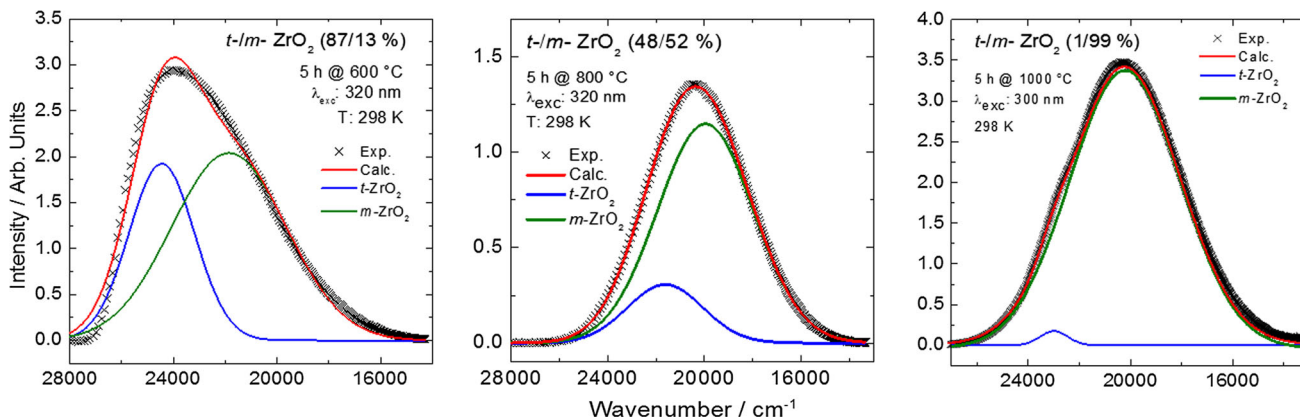


**Fig. 4** Emission spectra of ZrO<sub>2</sub> materials sintered at 600 (left), 800 (center) and 1000 °C (right). The deconvolution curves show two main contributions attributed to the t- and m-ZrO<sub>2</sub> phases. The calculated proportions of t/m-ZrO<sub>2</sub> is given in parenthesis

The energy balance is more favorable to charge transfer due to electrostatic attraction of the electron by the positive oxide vacancy,  $V_O^{\bullet\bullet}$  in Kröger–Vink notation [34] or  $F^{++}$  centre. The electron trapped in an oxide vacancy (now a  $F^+$  centre) and the hole in  $Ti^{IV}$  is, however, a metastable system and the relaxation occurs rather rapidly when the electron recombines with the hole. The energy then is transferred to the excited  $e_g$  levels of  $Ti^{3+}$  by multiphonon

relaxation. It should be noted that the annihilation of the metastable system depends also on the depth of the electron traps. Accordingly, the undoped ZrO<sub>2</sub> shows non-negligible persistent luminescence [22] probably due to bleaching of the deep traps. The emission bands of both the monoclinic and tetragonal ZrO<sub>2</sub> (Fig. 4) can be assigned to the  $3d^1(e_g \rightarrow t_{2g})$  transition of  $Ti^{3+}$  ion. The presence of different broad emission bands for the undoped ZrO<sub>2</sub>

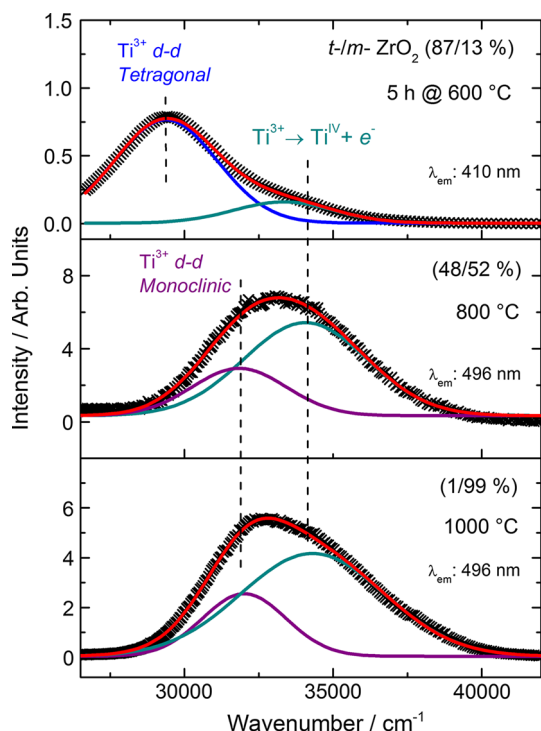


**Fig. 5** Deconvoluted excitation spectra of undoped  $\text{ZrO}_2$  materials obtained by sol–gel method and calcinated at different temperatures. The calculated proportions of *t*- and *m*- $\text{ZrO}_2$  are shown in parenthesis. All spectra were recorded at room temperature

materials is due to the different zirconia phases. This structural dependence can be related to a distorted  $\text{O}_h$  symmetry, the  $\text{TiO}_8$  cube for the tetragonal and the distorted  $\text{TiO}_7$  (monocapped) octahedron for the monoclinic phase [28]. The crystal field in the monoclinic form is expected to be weaker because of the fewer oxide ligands. All this in spite of the shorter Zr–O distances in the monoclinic form, values from 2.05 to 2.29 Å (average: 2.159 Å) while between 2.102 and 2.351 Å (average: 2.226 Å) have been reported for the monoclinic and tetragonal structures, respectively [26].

Owing to the weaker crystal field, the emission band of the  $e_g \rightarrow t_{2g}$  transition of  $\text{Ti}^{3+}$  ion for the monoclinic form, is redshifted when compared to the tetragonal phase. For the zirconia annealed at 600 °C, the tetragonal phase is predominantly present with 67–89 % of *t*- $\text{ZrO}_2$ , and an emission band in blue is observed due to the large crystal field splitting confirming this reasoning. The different processes leading to luminescence in undoped zirconia materials are schematized in a forthcoming section.

As stated above, the structure of the  $\text{ZrO}_2$  material depends not only on the annealing temperature but also on the *W* parameter. The annealed product contains in most cases both the monoclinic and the tetragonal forms of  $\text{ZrO}_2$ , i.e., a mixed structure product is obtained. However,

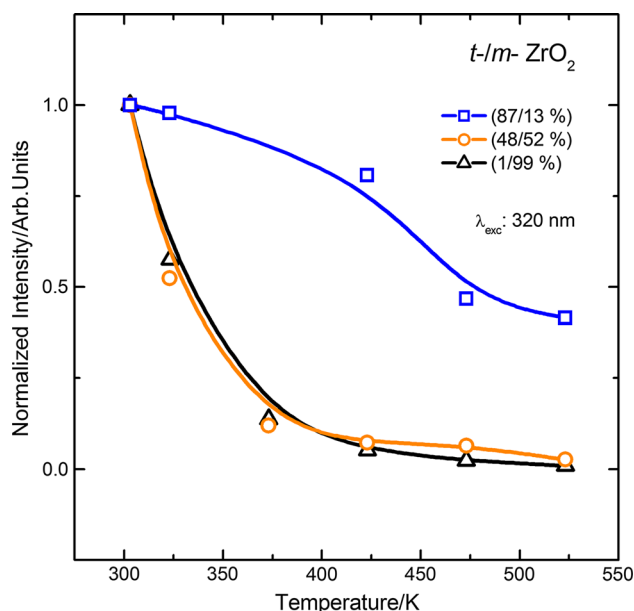


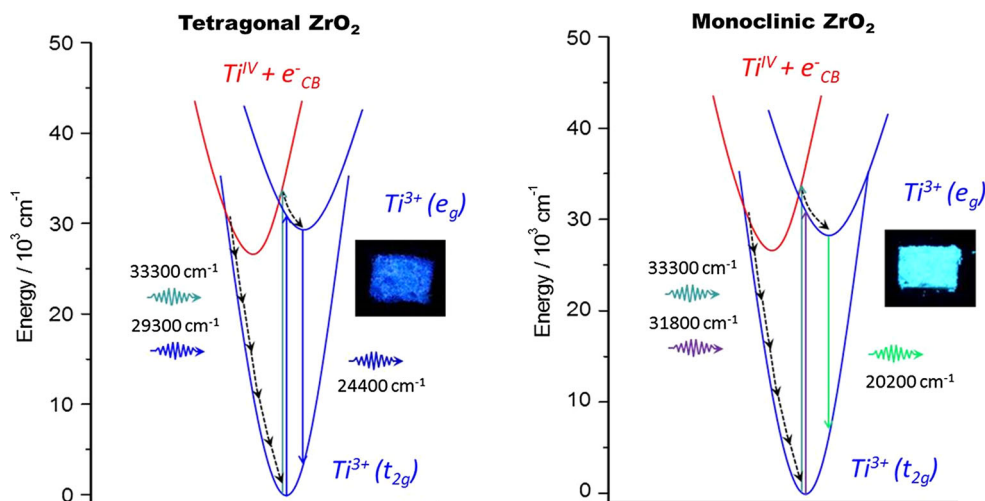
**Fig. 6** Integrated intensity of emission spectra as a function of temperature. The lines are just a guide to the eye

the deconvolution curves of the emission bands of  $\text{ZrO}_2$  can be used to probe the phase composition of the  $\text{ZrO}_2$  materials. The two emission bands can be separated and assigned to emission from the tetragonal [35] (ca.  $23000 \text{ cm}^{-1}$ ) and monoclinic phases (ca.  $20000 \text{ cm}^{-1}$ ). On the other hand, the compositions obtained from optical spectra do not match with those obtained from the X-ray diffraction for different reasons, for example the measuring temperature as discussed further below.

#### Thermal quenching of the luminescence of $\text{ZrO}_2$

The Fig. 6 shows the thermal quenching of the luminescence for the  $\text{ZrO}_2$  materials with different tetragonal/monoclinic proportions. The luminescence intensity of the monoclinic phase of the  $\text{ZrO}_2$  is quenched fast at lower temperatures to about half at temperatures close to 320 K (Fig. 6). This preliminary result shows that the thermal quenching is already effective at room temperature, which is confirmed by the low temperature emission spectra [17]. The same optical behavior is observed with the *t/m*- $\text{ZrO}_2$  (48/52 %) mixed material. The monoclinic contribution suffers the thermal quenching at lower temperatures hindering the luminescence output of the mixed materials. On the other hand, the thermal quenching of the tetragonal phase is less evident at room temperature and shows still 50 % intensity at temperatures at around 470 K. Both observations are in accordance with the Stokes shift observed in the materials.

**Fig. 7** Schematic presentation of excitation and emission processes for monoclinic and tetragonal undoped ZrO<sub>2</sub>



The tetragonal zirconia phase shows a smaller Stokes shift indicating less efficient non-radiative decay due to weaker vibrational contribution. The *m*-ZrO<sub>2</sub> phase shows larger Stokes shift and the thermal quenching is more operative at room temperature due to stronger vibrational contribution, converting the exciting energy into heat. Thus, the activation energy of the process is higher for *t*-ZrO<sub>2</sub> phase. As far as the practical applications are concerned, the different thermal behaviors of the two ZrO<sub>2</sub> phases can be used as thermally tunable phosphors.

**Emission diagram and tuning of luminescence**

As discussed in “Structural dependence of ZrO<sub>2</sub> photoluminescence” section, the different chemical environments for the Ti<sup>3+</sup> ion lead to different emission colors from *t*- and *m*-ZrO<sub>2</sub>, under UV radiation. The luminescence process depends on the following steps (Fig. 7): (i) The electron is UV-excited both to the *e<sub>g</sub>* level of Ti<sup>3+</sup> and to the oxide vacancies (V<sub>O</sub><sup>••</sup> or F<sup>++</sup> centers) in a *d–d* excitation and/or metal-to-ligand/host charge transfer (MLCT), (ii) The electron trapped in an oxide vacancy (F<sup>+</sup> centre) and the hole in Ti<sup>IV</sup> relax by electron–hole recombination and the energy is transferred to the excited *e<sub>g</sub>* levels of Ti<sup>3+</sup> by multiphonon relaxation and, (iii) The populated *e<sub>g</sub>* excited state decays to the *t<sub>2g</sub>* ground state, emitting photon with wavelength controlled by the 3d1 crystal field splitting.

Since the sol–gel method allows obtaining different mixtures of phases, only varying the *W* and temperature of calcination parameters, the emission colors could be fine tuned. This fact can be visualized in a chromaticity coordinate diagram of the emission from the zirconia materials with diverse phase compositions (Fig. 8). The different phase compositions at the same temperature show different emission colors arising from the zirconia materials.

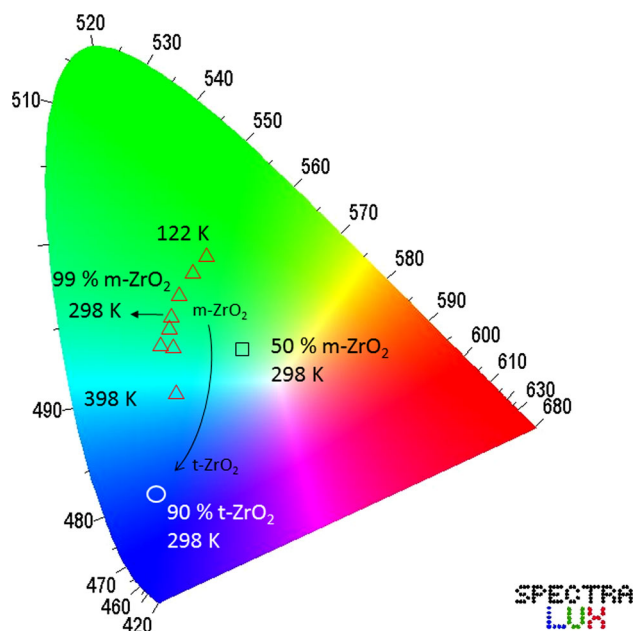


**Fig. 8** CIE chromaticity diagram for the emission from the 99 % *m*-ZrO<sub>2</sub> material recorded at different temperatures (red triangles), 90 % *t*-ZrO<sub>2</sub> (white circle) and 50 % *m*-ZrO<sub>2</sub> (black square) materials recorded at room temperature. The curved arrow indicates a tentative path connecting monoclinic to tetragonal zirconia (Color figure online)

Furthermore, the tetragonal and monoclinic phases of zirconia undergo thermal quenching at different temperatures, allowing tuning of the emission color, changing only the temperature of the material. For example, the material with 99 % of monoclinic phase shows a blue shift of the luminescence with the temperature varying from 122 to 398 K (spectra not shown). The materials with higher contents of the tetragonal phase do not show great change in the emission color as a function of temperature. These results show the great versatility of the undoped zirconia luminescent materials prepared by sol–gel method.

## Conclusions

The preparation of the sol–gel zirconia nanomaterials was studied systematically exploiting different parameters involved. Sets of interacting parameters were obtained which allowed a good control of the crystalline phases and morphology of the *t*-ZrO<sub>2</sub> and *m*-ZrO<sub>2</sub> nanomaterials. The sol–gel synthesis thus proved as a powerful method to obtain refractory materials with preferred photonic properties. Ti<sup>3+</sup> ion was assumed with success to be the luminescent activator in the undoped zirconia because most of the optical behavior of these nanomaterials could then be explained unambiguously. The materials have different emission, depending whether the phase is tetragonal, monoclinic, or mixed. The analytical deconvolution of the bands shows that the emission from tetragonal and monoclinic can be resolved and therefore the mixed material can be identified and their proportions qualitatively estimated. The persistent luminescence phenomenon suggested that the excitation probably involves the photoionization of Ti<sup>3+</sup> to Ti<sup>IV</sup> + e<sup>-</sup>. The relationship between the thermal quenching of the luminescence and the structure of each crystalline phase was studied and showed that tetragonal phase offers less non-radiative decay paths through multiphonon de-excitation. Photoluminescence and thermal quenching data suggest a mechanism of the photonic process in both *t*- and *m*-ZrO<sub>2</sub>. The *t*- and *m*-ZrO<sub>2</sub> materials are potentially applicable as structurally and thermally tunable luminescence materials. Zirconia can be used also as persistent luminescence materials or as a phosphor for thermometry, because of the lack of expensive starting materials—especially if juxtaposed to the rare earth based materials.

**Acknowledgements** Financial support is gratefully acknowledged from the Conselho Nacional de Desenvolvimento Científico e Tecnológico (CNPq) and the Academy of Finland through the Brazil-Finland Bilateral Project in the Photonics program, the Coordenação de Aperfeiçoamento de Pessoal de Nível Superior (CAPES), the Fundação de Amparo à Pesquisa do Estado de São Paulo (FAPESP), and the Instituto Nacional de Ciência e Tecnologia-Nanotecnologia para Marcadores Integrados (inct-INAMI).

## References

- Garvie RC (1975) Ceramic steel? *Nature* 258:703–704
- Wright PK, Evans AG (1999) Mechanisms governing the performance of thermal barrier coatings. *Curr Opin Solid State Mater Sci* 4:255–265. doi:10.1016/S1359-0286(99)00024-8
- Li CW, McKerns MM, Fultz B (2011) A Raman spectrometry study of phonon anharmonicity of zirconia at elevated temperatures. *J Am Ceram Soc* 94:224–229. doi:10.1111/j.1551-2916.2010.04057.x
- Hyppänen I, Hölsä J, Kankare J et al (2008) Defect structure and up-conversion luminescence properties of ZrO<sub>2</sub>:Yb<sup>3+</sup>, Er<sup>3+</sup> nanomaterials. *J Fluoresc* 18:1029–1034. doi:10.1007/s10895-008-0327-0
- Gallino F, Di Valentin C, Pacchioni G (2011) Band gap engineering of bulk ZrO<sub>2</sub> by Ti doping. *Phys Chem Chem Phys* 13:17667–17675. doi:10.1039/c1cp21987a
- Fan Z, An J, Iancu A, Prinz FB (2012) Thickness effects of yttria-doped ceria interlayers on solid oxide fuel cells. *J Power Sources* 218:187–191. doi:10.1016/j.jpowsour.2012.06.103
- Zhou R, Jiang X, Mao J, Zheng X (1997) Oxidation of carbon monoxide catalyzed by copper–zirconium composite oxides. *Appl Catal A Gen* 162:213–222. doi:10.1016/S0926-860X(97)00099-9
- Tanabe K, Yamaguchi T (1994) Acid–base bifunctional catalysis by ZrO<sub>2</sub> and its mixed oxides. *Catal Today* 20:185–198. doi:10.1016/0920-5861(94)80002-2
- Garvie RC (1965) The occurrence of metastable tetragonal zirconia as a crystallite size effect. *J Phys Chem* 69:1238–1243. doi:10.1021/j100888a024
- Foster AS, Sulimov VB, Gejo FL et al (2001) Structure and electrical levels of point defects in monoclinic zirconia. *Phys Rev* 64:1–10. doi:10.1103/PhysRevB.64.224108
- Srinivasan R, Hubbard CR, Cavin OB, Davis BH (1993) Factors determining the crystal phases of zirconia powders: a new outlook. *Chem Mater* 5:27–31. doi:10.1021/cm00025a009
- Reisfeld R, Zelner M, Patra A (2000) Fluorescence study of zirconia films doped by Eu<sup>3+</sup>, Tb<sup>3+</sup> and Sm<sup>3+</sup> and their comparison with silica films. *J Alloys Compd* 301:147–151. doi:10.1016/S0925-8388(99)00714-8
- Smits K, Grigorjeva L, Millers D et al (2010) Europium doped zirconia luminescence. *Opt Mater* 32:827–831. doi:10.1016/j.optmat.2010.03.002
- Malyi OI, Chen Z, Shu GG, Wu P (2011) Effect of sulfur impurity on the stability of cubic zirconia and its interfaces with metals. *J Mater Chem* 21:12363. doi:10.1039/c1jm10908a
- López-luke T, De la Rosa E, Romero VH et al (2011) Solvent and surfactant effect on the self-assembly and luminescence properties of ZrO<sub>2</sub>:Eu<sup>3+</sup> nanoparticles. *Appl Phys B* 102:641–649. doi:10.1007/s00340-010-4233-1
- Hemmer E, Soga K, Konishi T et al (2010) Influence of the host phase on the vibrational spectra of europium-doped zirconia prepared by hydrothermal processing. *J Am Ceram Soc* 11:3873–3879. doi:10.1111/j.1551-2916.2010.03981.x
- Harrison DE, Melamed NT, Subbarao EC (1963) A new family of self-activated phosphors. *J Electrochem Soc* 110:23. doi:10.1149/1.2425665
- Hahn R, Berger S, Schmuki P (2010) Bright visible luminescence of self-organized ZrO<sub>2</sub> nanotubes. *J Solid State Electrochem* 14:285–288. doi:10.1007/s10008-008-0748-3
- Sarver JF (1966) Preparation and luminescent properties of Ti-activated zirconia. *J Electrochem Soc* 133:124–128. doi:10.1149/1.2423883
- Phatak GM, Gangadharan K, Pal H, Mittal JP (1994) Luminescence properties of Ti-doped gem-grade zirconia powders. *Bull Mater Sci* 17:163–169. doi:10.1007/BF02747563
- Cong Y, Li B, Wang X et al (2008) Synthesis and optical property studies of nanocrystalline ZrO<sub>2</sub>:Ti long-lasting phosphors. *J Electrochem Soc* 155:195–198. doi:10.1149/1.2971023
- Carvalho JM, Rodrigues LCV, Hölsä J et al (2012) Influence of titanium and lutetium on the persistent luminescence of ZrO<sub>2</sub>. *Opt Mater Express* 2:331–340. doi:10.1364/OME.2.000331
- Hench LL, West JK (1990) The sol–gel process. *Chem Rev* 90:33–72. doi:10.1021/cr00099a003
- Toraya H, Yoshimura M, Somiya S (1984) Calibration curve for quantitative analysis of the monoclinic-tetragonal ZrO<sub>2</sub> system by X-ray diffraction. *Commun Am Ceram Soc* 67:119–121
- Pan M, Liu J, Lu M et al (2001) Preparation of zirconia xerogels and ceramics by sol–gel method and the analysis of their thermal behavior. *Thermochim Acta* 376:77–82. doi:10.1016/S0040-6031(01)00536-6

26. Howard CJ, Hill RJ, Reichert BE (1988) Structures of the  $ZrO_2$  polymorphs at room temperature by high-resolution neutron powder diffraction. *Acta Crystallogr B* 44:116–120. doi:10.1107/S0108768187010279
27. Zhao J, Fan W, Wu D, Sun Y (2000) Synthesis of highly stabilized zirconia sols from zirconium n-propoxide-diglycol system. *J Non Cryst Solids* 261:15–20. doi:10.1016/S0022-3093(99)00651-1
28. Chen S-G, Yin Y-S, Wang D-P, Li J (2004) Reduced activation energy and crystalline size for yttria-stabilized zirconia nanocrystals: an experimental and theoretical study. *J Cryst Growth* 267:100–109. doi:10.1016/j.jcrysgro.2004.03.017
29. Vegard L (1921) Die Konstitution de Mischkristalle und die Raumbfüllung der Atome. *Zeitschrift für Phys* 5:17–26. doi:10.1007/BF01349680
30. Moon C, Masayuki N, Miura K, Hirao K (2009) Blue long-lasting phosphorescence of Ti-doped  $BaZrO_3$  perovskites. *J Lumin* 129:817–819. doi:10.1016/j.jlumin.2009.03.002
31. Andrade LHC, Lima SM, Novatski A et al (2008) Long fluorescence lifetime of  $Ti^{3+}$ -doped low silica calcium aluminosilicate glass. *Phys Rev Lett* 100:027402. doi:10.1103/PhysRevLett.100.027402
32. Andrade LHC, Lima SM, Novatski A et al (2008) Spectroscopic assignments of  $Ti^{3+}$  and  $Ti^{4+}$  in titanium-doped  $OH^-$  free low-silica calcium aluminosilicate glass and role of structural defects on the observed long lifetime and high fluorescence of  $Ti^{3+}$  ions. *Phys Rev B* 78:224202. doi:10.1103/PhysRevB.78.224202
33. Iwasaki K, Takahashi Y, Masai H, Fujiwara T (2009) Blue photoluminescence, greenish-blue afterglow and their Ti-concentration dependence in rare earth-free bazirite-type  $BaZr_{1-x}Ti_xSi_3O_9$ . *Opt Express* 17:18054–18062. doi:10.1364/OE.17.018054
34. Kröger FA, Vink HJ (1958) Relations between the concentrations of imperfections in solids. *J Phys Chem Solids* 5:208–223
35. Smits K, Grigorjeva L, Millers D et al (2011) Intrinsic defect related luminescence in  $ZrO_2$ . *J Lumin* 131:2058–2062. doi:10.1016/j.jlumin.2011.05.018